

Germline-Activating *RRAS2* Mutations Cause Noonan Syndrome

Tetsuya Niihori,^{1,2,*} Koki Nagai,¹ Atsushi Fujita,³ Hirofumi Ohashi,⁴ Nobuhiko Okamoto,⁵ Satoshi Okada,⁶ Atsuko Harada,⁷ Hirotaka Kihara,⁸ Thomas Arbogast,² Ryo Funayama,⁹ Matsuyuki Shirota,¹⁰ Keiko Nakayama,⁹ Taiki Abe,¹ Shin-ichi Inoue,¹ I-Chun Tsai,² Naomichi Matsumoto,³ Erica E. Davis,^{2,*} and Yoko Aoki¹

Noonan syndrome (NS) is characterized by distinctive craniofacial appearance, short stature, and congenital heart disease. Approximately 80% of individuals with NS harbor mutations in genes whose products are involved in the RAS/mitogen-activating protein kinase (MAPK) pathway. However, the underlying genetic causes in nearly 20% of individuals with NS phenotype remain unexplained. Here, we report four *de novo* *RRAS2* variants in three individuals with NS. *RRAS2* is a member of the RAS subfamily and is ubiquitously expressed. Three variants, c.70_78dup (p.Gly24_Gly26dup), c.216A>T (p.Gln72His), and c.215A>T (p.Gln72Leu), have been found in cancers; our functional analyses showed that these three changes induced elevated association of RAF1 and that they activated ERK1/2 and ELK1. Notably, prominent activation of ERK1/2 and ELK1 by p.Gln72Leu associates with the severe phenotype of the individual harboring this change. To examine variant pathogenicity *in vivo*, we generated zebrafish models. Larvae overexpressing c.70_78dup (p.Gly24_Gly26dup) or c.216A>T (p.Gln72His) variants, but not wild-type *RRAS2* RNAs, showed craniofacial defects and macrocephaly. The same dose injection of mRNA encoding c.215A>T (p.Gln72Leu) caused severe developmental impairments and low dose overexpression of this variant induced craniofacial defects. In contrast, the *RRAS2* c.224T>G (p.Phe75Cys) change, located on the same allele with p.Gln72His in an individual with NS, resulted in no aberrant *in vitro* or *in vivo* phenotypes by itself. Together, our findings suggest that activating *RRAS2* mutations can cause NS and expand the involvement of *RRAS2* proto-oncogene to rare germline disorders.

Noonan syndrome (NS [MIM: 163950]) is an autosomal-dominant or -recessive disorder characterized by distinctive craniofacial features, short stature, and congenital heart disease.^{1,2} NS is one of the developmental syndromes caused by mutations in molecules involved in the RAS/MAPK (RAF/MEK/ERK) signaling pathway, termed collectively as the RASopathies.³ The RAS/MAPK pathway regulates cell proliferation, differentiation, survival, and apoptosis.⁴ Previous studies of genes associated with NS and related disorders, including Costello syndrome (CS [MIM: 218040]) and cardio-facio-cutaneous syndrome (CFCS [MIM: 115150]),^{5–9} have unified these clinically overlapping disorders as RASopathies in which dysregulation of the RAS/MAPK pathway is a common molecular basis. To date, mutations in genes encoding many components of the RAS/MAPK pathway, including *PTPN11* (MIM: 176876), *KRAS* (MIM: 190070), *SOS1* (MIM: 182530), *RAF1* (MIM: 164760), *SHOC2* (MIM: 602775), *CBL* (MIM: 165360), *BRAF* (MIM: 164757), *NRAS* (MIM: 164790), *RRAS* (MIM: 165090), have been reported as causes of NS or NS-like syndromes.¹

The emergence of whole-exome sequencing (WES) has accelerated the discovery of RASopathy genes. We identified

RIT1 (MIM: 609591) mutations in individuals with NS using WES.¹⁰ Subsequently, mutations in *A2ML1* (MIM: 610627), *RASA2* (MIM: 601589), *SOS2* (MIM: 601247), *LZTR1* (MIM: 600574),¹ *PPP1CB* (MIM: 600590),¹¹ and *MRAS* (MIM: 608435)¹² have been reported as causes of NS or NS-like syndromes, although the contribution of each locus to the pathogenicity of NS is modest. Such discoveries suggest that the remaining ~20% of individuals with NS that remain undiagnosed molecularly will likely harbor rare, possibly private, mutations in a host of hitherto uncharacterized genes. As such, we have undertaken an investigational paradigm in which we pair WES on individuals with NS-related disorders with *in vitro* and *in vivo* studies of candidate pathogenic variants. In the present study, we report the identification of three individuals with *de novo* *RRAS2* (MIM: 600098) variants. Our genetic and functional data support a causal role for *de novo* dominant alleles as drivers of NS-like pathology in humans.

First, we performed WES on 27 individuals with clinically diagnosed or suspected NS or NS-related disorders without known RASopathy mutations (details in [Supplemental Material and Methods](#)). This study was approved by the Ethics Committee of the Tohoku University School

¹Department of Medical Genetics, Tohoku University School of Medicine, Sendai 980-8574, Japan; ²Center for Human Disease Modeling, Duke University Medical Center, Durham, NC 27701, USA; ³Department of Human Genetics, Yokohama City University Graduate School of Medicine, Yokohama 236-0004, Japan; ⁴Division of Medical Genetics, Saitama Children's Medical Center, Saitama 330-8777, Japan; ⁵Department of Medical Genetics, Osaka Women's and Children's Hospital, Osaka 594-1101, Japan; ⁶Department of Pediatrics, Hiroshima University Graduate School of Biomedical & Health Sciences, Hiroshima 734-8551, Japan; ⁷Department of Pediatric Neurosurgery, Takatsuki General Hospital, Osaka 569-1192, Japan; ⁸Department of Pediatrics, Onomichi General Hospital, Hiroshima 722-8508, Japan; ⁹Department of Cell Proliferation, United Center for Advanced Research and Translational Medicine, Tohoku University Graduate School of Medicine, Sendai 980-8575, Japan; ¹⁰Division of Interdisciplinary Medical Sciences, United Center for Advanced Research and Translational Medicine, Tohoku University Graduate School of Medicine, Sendai 980-8575, Japan

*Correspondence: tniihori@med.tohoku.ac.jp (T.N.), katsanis@cellbio.duke.edu (N.K.)

<https://doi.org/10.1016/j.ajhg.2019.04.014>

© 2019 American Society of Human Genetics.



Table 1. Clinical Features in the Scoring System of Noonan Syndrome Proposed by van der Burgt¹⁵ in Individuals with *RRAS2* Mutations

Individual	NS462	NS833	HU1
Sex	female	female	male
Age at evaluation	6 years	4 years	3 years
Initial diagnosis	NS or CFC	NS	undiagnosed
<i>RRAS2</i> variant	c.70_78dup (p.Gly24_Gly26dup)	c.[216A>T;224T>G], p.[(Gln72His);(Phe75Cys)]	c.215A>T (p.Gln72Leu)
Facial dysmorphology	typical	typical	suggestive
Cardiac feature	pulmonic stenosis	–	dilated cardiomyopathy
Short stature (SD)	– (+0.2)	+ (–2.4)	+ (–5.9)
Pectus abnormalities	–	pectus excavatum	pectus excavatum
Family history	simplex	simplex	simplex
Intellectual disability (ID), cryptorchidism, and lymphatic dysplasia	–	mild ID	severe ID, cryptorchidism

of Medicine. Written informed consent was obtained from all subjects involved in the study or from their parents. We filtered the identified variants by minor allele frequency (MAF) in population databases such as 1000 Genomes, dbSNP, ExAC Browser, and Human Genetic Variation Database (absent or <0.01) and by functional prediction (missense, nonsense, indel, or splicing). We prioritized genes whose products are members of the RAS/MAPK pathway. We found a *RRAS2* (GenBank: NM_012250.6; c.70_78dup) variant in individual NS462 and two *RRAS2* variants (c.216A>T and c.224T>G) in individual NS833 (Table 1). Segregation analysis in the parents revealed that all three variants arose *de novo*. Parentage in each family was confirmed by the thousands of variants in common between child and parent in the trio exomes. *RRAS2*, also called *TC21*, encodes a member of the RAS GTPase superfamily and is expressed ubiquitously, with the highest levels in the heart, placenta, and skeletal muscle.¹³ *RRAS2* is an evolutionarily conserved protein and exhibits 55% amino acid identity to RAS proteins.¹⁴

Subsequently, we sequenced all coding exons of *RRAS2* in 191 molecularly undiagnosed individuals suspected of having NS or NS-related disorders, but we did not identify any additional rare (i.e., <0.01 MAF in population databases) nonsynonymous variants. In parallel, we performed WES on samples from an undiagnosed individual HU1 with severe failure to thrive and his healthy parents. We identified a *de novo* *RRAS2* c.215A>T variant in HU1 and confirmed the segregation of the variant by Sanger sequencing. The c.215A>T (p.Gln72Leu) variant has been found in epithelial ovarian tumors,¹³ juvenile myelomonocytic leukemia,¹⁵ and other cancers (reported in COSMIC: COSG1128). Importantly, the codon Gln72 corresponds to codon Gln61 in *KRAS*, *HRAS*, and *NRAS*, a hotspot for mutations in several cancers (Figures 1A–1C).¹⁶ This variant has also been reported to induce activation of ERK¹⁷ and to elevate neoplastic transformation.^{13,17} Individual HU1 was 3 years old at the time of last examination and was the third

child of non-consanguineous parents. He had short stature, pectus excavatum, intellectual disability, and cryptorchidism (Supplemental Note; Tables 1 and S1). His facial appearance was not typical for NS at age 3 years, however, retrospective inspection of the images taken in his infancy revealed that he had a facial gestalt of NS. Therefore, he fulfilled the criteria for NS proposed by van der Burgt.¹⁸ In total, we identified rare *RRAS2* variants in 3 of 219 individuals suspected of having NS or NS-related disorders. These data suggest that, similar to other recently discovered NS-associated genes, *RRAS2* mutations likely account for a small fraction of NS.

Individual NS462, who harbored *RRAS2* c.70_78dup, was 6 years old at her last clinical examination; she is the second child of healthy non-consanguineous parents. She presented with macrocephaly, pulmonic stenosis, hemangiomas, mild myopia, and left hearing impairment (Tables 1 and S1). Microarray analysis did not reveal gross duplication or deletion. Her initial diagnosis was CFCS or NS. *RRAS2* c.70_78dup, which encodes p.Gly24_Gly26dup, maps to a phosphate-binding loop (P loop) in a domain that is conserved across the RAS family (Figures 1A–1C). This duplication has already been identified in a human uterine leiomyosarcoma cell line, SK-UT-1,¹⁹ and it is known to activate ERK²⁰ and its transforming activity.¹⁹ We also sequenced DNA from the individual's hair and fingernails and confirmed the presence of *RRAS2* c.70_78dup, suggesting that the variation was not a somatic mutation in peripheral blood (data not shown).

Individual NS833 was 4 years old at the time of last examination, and she is the first child of healthy non-consanguineous parents. She presented with macrocephaly with enlarged ventricles, short stature (–2.4 SD), pectus excavatum, skin manifestations, and mild intellectual disability (Figures 1D and 1E; Tables 1 and S1). She was diagnosed with NS at 2 years 4 months. WES detected two *RRAS2* variants, c.216A>T and c.224T>G. Sanger sequencing confirmed the presence of c.216A>T and c.224T>G in

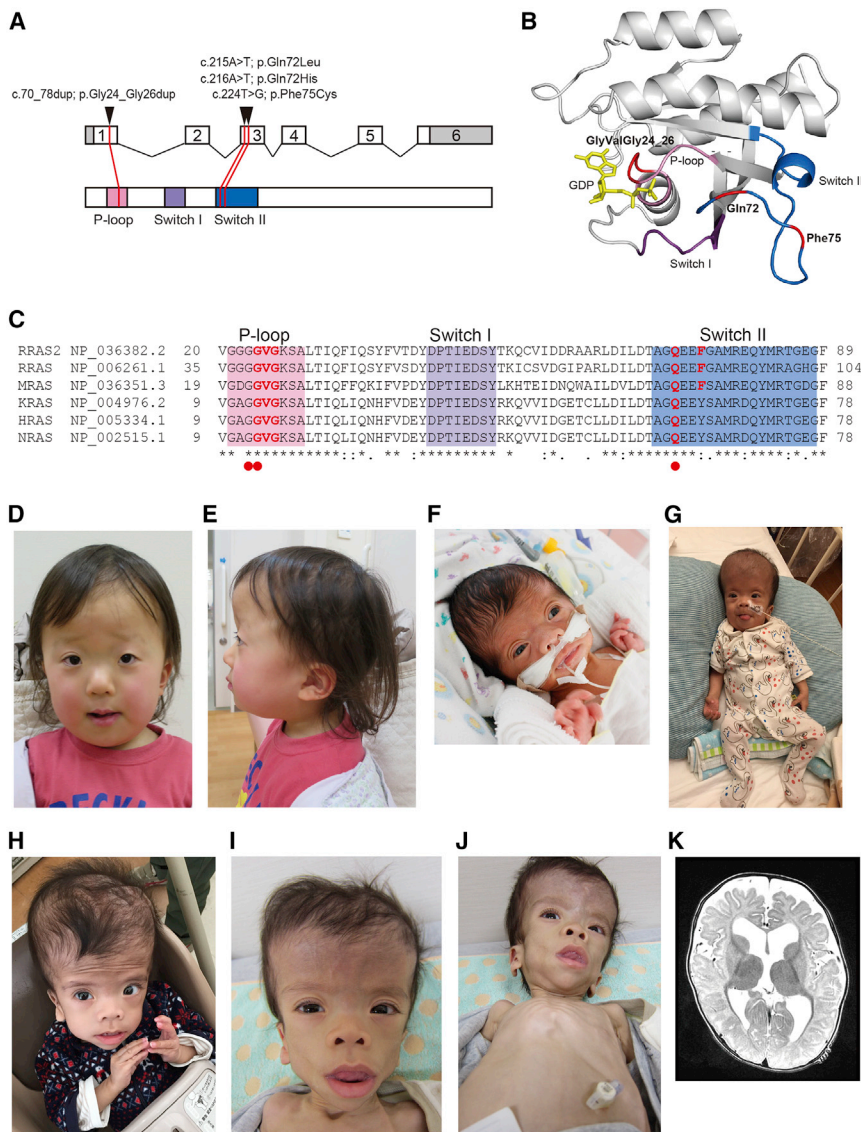


Figure 1. *RRAS2* Mutations Identified in Individuals with Noonan Syndrome

(A) Exon-intron structure of *RRAS2* (upper) and functional domains of *RRAS2* proteins (lower). *RRAS2* variants in individuals with Noonan syndrome (NS) were located in phosphate-binding loop or switch II region. (B) Crystal structure of human *RRAS2*. Phosphate-binding loop, switch I, switch II, GDP, and residues mutated in individuals with Noonan syndrome (NS) are highlighted in pink, purple, blue, yellow, and red, respectively.

(C) Partial amino acid sequence alignment of human *RRAS2*, *RRAS*, *MRAS*, *KRAS*, *HRAS*, and *NRAS*. High conservation of residues of Gly24-Gly26 and Gln72 through all paralogs are shown. Conservation of residues at Phe75 was limited in the *RRAS* subfamily. Red circles indicate hotspot residues mutated in various cancers in *KRAS*, *HRAS*, and *NRAS*.

(D and E) Photos of individual NS833. She had the definitive facial appearance of NS at 4 years of age.

(F–J) Photos of individual HU1 at (F) neonatal period, (G) 7 months, (H) 22 months, and (I and J) 3 years of age.

(K) Axial slice of brain magnetic resonance image of HU1 taken at 6 months of age shows ventriculomegaly and widened subarachnoid spaces in the frontal and temporal lobes.

the same allele in NS833 (Figure S1). The c.216A>T (p.Gln72His) variant has been found in endometrioid carcinoma (reported in COSMIC: COSG1128) and results in an amino acid change at the same residue as p.Gln72Leu, which activates ERK. In contrast, c.224T>G (p.Phe75Cys) has not been reported thus far. In this context, we presumed that aberrant activation of the RAS/MAPK pathway underlies NS of the individuals with *RRAS2* variants.

To test the pathogenicity of the discovered *RRAS2* mutations, we performed pull-down assays with the Raf-Ras-binding domain (RBD, residues 1–149) of RAF1.²¹ We transfected a *RRAS2* wild-type (WT) or mutant cDNAs in HEK293 cells and pulled-down activated RAS. The *RRAS2* levels in cells expressing p.[Gln72His;Phe75Cys] and p.Phe75Cys were decreased compared to WT (consistent results across three independent experiments). Furthermore, compared to WT *RRAS2* we observed increased binding of activated RAS for each of *RRAS2* p.Gly24_Gly26dup, p.[Gln72His;Phe75Cys], p.Gln72His, and p.Gln72Leu but not p.Phe75Cys alone, suggesting that the first four alleles

are pathogenic but that the fifth is benign (Figure 2A). Next, we conducted immunoblotting of the cell lysates expressing WT or mutant *RRAS2* using anti-phospho-MEK1/2 and phospho-ERK1/2 antibodies. We observed increased levels of phospho-MEK1/2 and phospho-ERK1/2 in the cells expressing *RRAS2* p.Gly24_Gly26dup, p.[Gln72His;Phe75Cys], p.Gln72His, and p.Gln72Leu. These results suggest that p.Gly24_Gly26dup, p.[Gln72His;Phe75Cys], p.Gln72His, and p.Gln72Leu mutants had increased affinity toward RAF and activate MEK/ERK.

Our pull-down assays and immunoblotting data suggested downstream activation of the RAS/MAPK pathway. To confirm these findings, we performed reporter assays using ELK-1, a transcriptional factor downstream of RAS/MAPK, whose transactivation in cells expressing RASopathy-gene mutations is known to increase.⁵ We transfected HEK293 cells with WT or mutant *RRAS2* expression constructs, a pFR-luc trans-reporter vector, a pFA2-ELK1 vector, and a phRLnull-luc vector and measured their relative luciferase activity (RLA). Consistent with our earlier data, we observed a significant increase in RLA in cells transfected with *RRAS2* p.Gly24_Gly26dup, p.[Gln72His;Phe75Cys], p.Gln72His, and p.Gln72Leu but not in cells transfected with p.Phe75Cys alone (Figure 2B). These results suggest that *RRAS2* p.Gly24_Gly26dup,

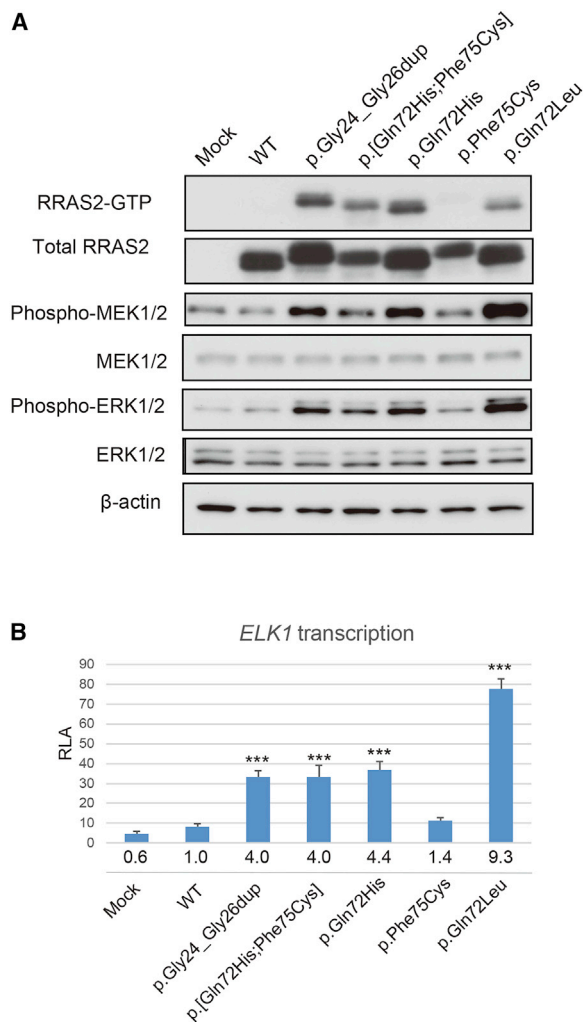


Figure 2. Functional Assays of *RRAS2* Variants

(A) Representative immunoblots of three independent experiments. HEK293 cells transfected with WT or mutant *RRAS2* constructs or empty vector (Mock) were used for pull-down assays and immunoblotting. *RRAS2*-guanosine triphosphate (GTP) which was pulled down using RAF1-RBD agarose, total *RRAS2*, phospho-MEK1/2, total MEK1/2, phospho-ERK1/2, total ERK1/2, and β -actin as a loading control were shown. WT, wild-type.

(B) Stimulation of *ELK1* transcription by *RRAS2* mutants. *ELK1*-GAL4 and GAL4-luciferase trans-reporter vectors were transiently co-transfected with *RRAS2* constructs into unstimulated HEK293 cells. Relative luciferase activity (RLA) was normalized to the activity of a co-transfected control vector (phRLnull-luc) expressing *Renilla reniformis* luciferase. Folds under each bar were calculated as a multiple of WT. Data are presented as mean \pm SD; $n = 3$ per group. WT, wild-type. *** $p < 0.001$ compared with WT.

p.[Gln72His;Phe75Cys], p.Gln72His, and p.Gln72Leu as well as other RASopathy mutations stimulate the signaling pathway leading to *ELK1* activation.

Our *in vitro* data suggest that aberrant activation of RAS/MAPK are likely drivers of the pathology seen in our NS-affected case subjects. To test this model *in vivo*, we turned to zebrafish, a useful model for testing defective RAS signaling,^{22–24} whose genome also contains a *rras2* ortholog (96% identical; 98% similar for human versus zebrafish protein). We took advantage of the fact that quan-

titative measurements of the craniofacial skeleton demarcated by a transgene expressing GFP under the *coll1a1* promoter Tg(-1.4*coll1a1:egfp*) are a useful method for assessing the effect of alleles that impact craniofacial development.²⁵ Given the *in vitro* data, we asked whether expression of each of the human *RRAS2* mutant mRNAs might recapitulate aspects of pathology observed in affected individuals. To test this possibility, we injected WT mRNA of human *RRAS2* or mRNA encoding each of the variants (or combination thereof) into transgenic embryos. We noticed that injection of 25 pg of p.Gln72Leu mRNA was lethal, but injections of the same dose of WT or the other mutant mRNAs represented the highest non-lethal dose. Therefore, we started with embryos which were injected with 25 pg of WT or mutant mRNA except for p.Gln72Leu. At 11 h post fertilization (hpf), we observed significant elongation of the yolk in *RRAS2* p.Gly24_Gly26dup, p.[Gln72His;Phe75Cys], and p.Gln72His embryos compared to WT (Figure S2); differences between p.Phe75Cys and WT were not significant. We then raised embryos to 3 days post fertilization (dpf) and measured the ceratohyal angle, a mandibular structure which reflects the width and bluntness of the head.²⁶ The ceratohyal angle was significantly increased in larval batches injected with mRNA encoding p.Gly24_Gly26dup, p.[Gln72His;Phe75Cys], and p.Gln72His (Figures 3A and 3B) but was indistinguishable from WT upon injection of p.Phe75Cys mRNA. These results were consistent with our *in vitro* data and prior genetic observations in tumors, all of which point toward the mutants driving hyperactivation of MAPK signaling.

As a second test, we also measured body length and relative head length (head length divided by body length) at 3 dpf. Expression of *RRAS2* p.Gly24_Gly26dup, p.[Gln72His;Phe75Cys], and p.Gln72His led to significant decreases in body length compared to WT *RRAS2* (Figures 3C and 3D). Relative head length in *RRAS2* p.Gly24_Gly26dup, p.[Gln72His;Phe75Cys], and p.Gln72His larvae were also greater than in WT larvae (Figure 3E). Finally, we also observed an increased incidence of pericardial effusion in *RRAS2* p.Gly24_Gly26dup, p.[Gln72His;Phe75Cys], and p.Gln72His larvae (Figure S3) that might underscore a structural heart defect.

To test the p.Gln72Leu variant, we established the highest tolerated dose of mRNA and injected it into embryos to observe developmental defects in live larvae. The embryos injected with 5 pg of p.Gln72Leu mRNA were viable and showed significantly increased ceratohyal angles compared to the uninjected controls (Figure 3B, right), although the body length and relative head size of p.Gln72Leu-injected larvae were not different from those of uninjected controls (right panels of Figures 3D and 3E). Together, these data suggest that expression of *RRAS2* encoding p.Gly24_Gly26dup, p.[Gln72His;Phe75Cys], p.Gln72His, and p.Gln72Leu induced craniofacial patterning defects in zebrafish larvae that correspond to symptoms relevant to our affected individuals and further support our *in vitro* studies.

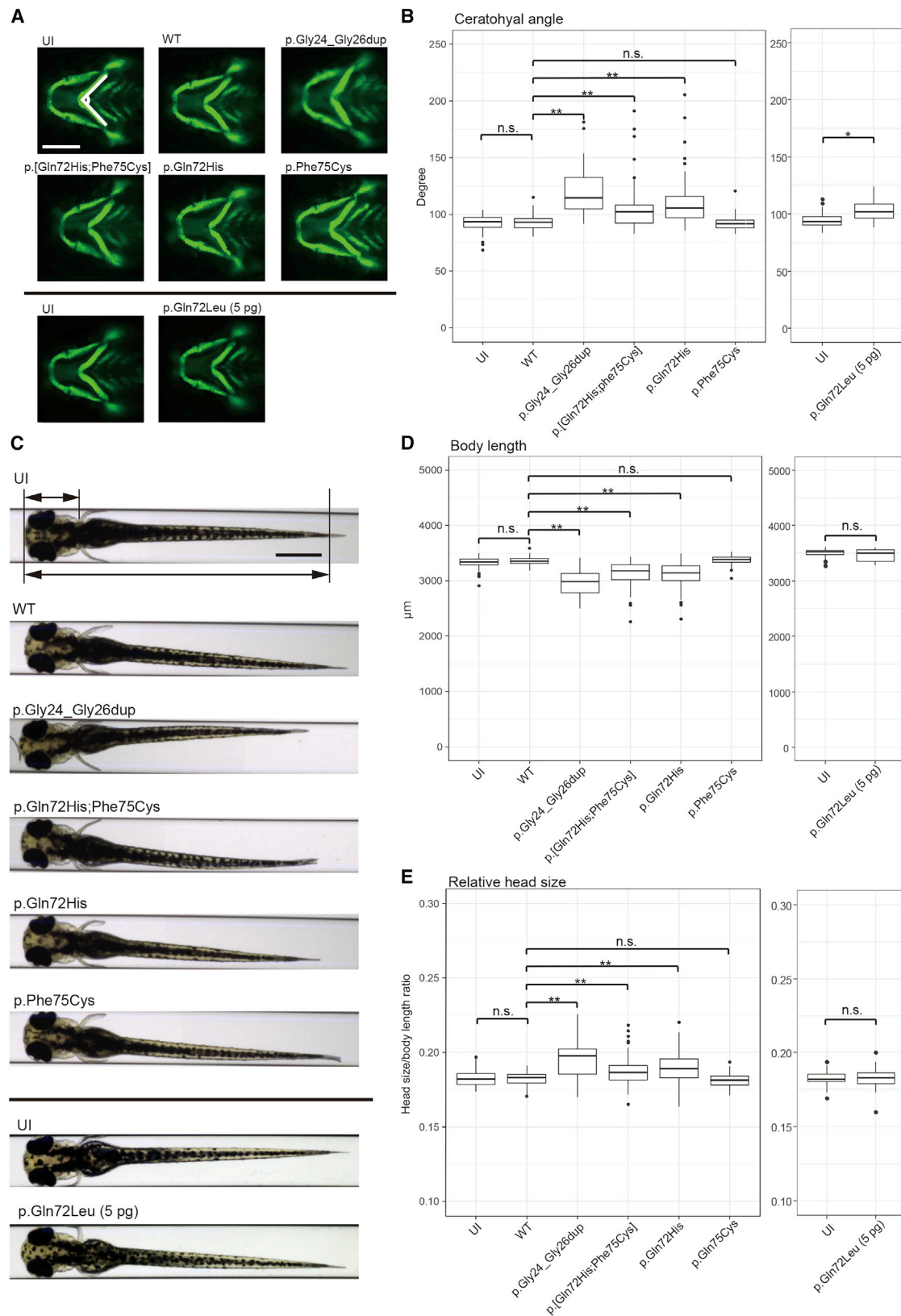


Figure 3. Morphology of Zebrafish Larvae Injected with Wild-Type (WT) or Mutant *RRAS2* mRNA at 3 Days Post Fertilization (dpf)

(A) Tg(-1.4*coll1a1:egfp*) transgenic embryos, in which cartilage cells are marked by EGFP, were injected at the 1- to 4-cell stage with RNA encoding *RRAS2*-WT or variants identified in affected individuals. The angle of the ceratohyal cartilage was measured at 3 dpf. Representative images of an uninjected control (UI) and *RRAS2*-variant mRNA injected larvae are depicted. Scale bar: 200 μ m.

(legend continued on next page)

We describe *de novo* *RRAS2* mutations identified in three individuals showing a NS phenotype. All three individuals with *RRAS2* mutations had macrocephaly and typical or suggestive facial appearance of NS. Regarding the other features, they had clinical manifestations sufficient to fulfill the diagnostic criteria by van der Burgt, though they were not common among all individuals. HU1, who had more severe phenotype such as failure to thrive and severe developmental delay, harbored a p.Gln72Leu variant. This variant elicited a potent effect in our *in vitro* and *in vivo* assays, suggesting a possible genotype-phenotype correlation. However, the identification of a larger *RRAS2* allelic series will be required to enable establishment of such correlations.

Individual NS833 has two *de novo* variants, p.Gln72His and p.Phe75Cys, in *cis*. p.Gln72His has been found in endometrioid carcinoma and is likely pathogenic because of its homologous position to the hotspot Gln61 in *KRAS*, *NRAS*, and *HRAS*.¹⁶ Our functional data agree with that prediction. In contrast, the second variant is likely benign. Multiple *in silico* analyses predicted that p.Phe75Cys exerts an adverse effect (Table S2), which is only partially consistent with our functional analyses wherein we observe decreased protein levels compared to WT. It is formally possible that this variant is detrimental to protein function but not in a fashion that would give rise to NS-associated pathologies, especially since the allele is absent from population databases.

Our zebrafish model expressing *RRAS2* mutations showed elongated shapes of developing embryos, reduced body length, macrocephaly, and craniofacial defects. Injection of the same dose of p.Gln72Leu mRNA as those of the other variants induced embryonic death, suggesting stronger impact of this mutation. We observed significant differences in ceratohyal angle in larvae with lower dose injection of p.Gln72Leu mRNA, but not in body length and relative head size. Increases of ceratohyal angle may be a sensitive marker in zebrafish models of RASopathies. Zebrafish models expressing *BRAF*, *HRAS* (MIM: 190020), and *PTPN11* mutations were approved for functional studies by ClinGen's RASopathy Expert Panel.²⁷ Notably, craniofacial defects, including wide heads and/or hypoplasia of the ventral side of the head, have been observed in zebrafish models expressing *PTPN11*,²⁸ *HRAS*,²⁹ *NRAS*,²⁶ *RIT1*,¹⁰ and zebrafish *a2ml1*³⁰ mutations. Furthermore, elongation of developing embryos at 10–12 hpf has

been reported in zebrafish models of RASopathies expressing *BRAF*, *MAP2K1* (MIM: 176872), *MAP2K2* (MIM: 601263),³¹ *RIT1*,¹⁰ and *NRAS*.²⁶ In addition, reduced body length has been seen in zebrafish models expressing *PTPN11*²⁸ and *HRAS*²⁹ mutations. Such similarities among RASopathy models suggest common underlying mechanisms led by the dysregulation of the RAS/MAPK pathway.

In summary, we identified four *de novo* *RRAS2* variants in three individuals with NS, three of which are likely drivers of pathology through the hyperactivation of the RAS/MAPK pathway. Together with an accompanying study showing *RRAS2* mutations in individuals with NS or NS-like phenotype,³² these findings broaden our understanding of roles of *RRAS2* in human development, expanding the mutational landscape of NS and related disorders. Our work also highlights how, given the rarity of the remaining genes for this group of disorders, the combination of genetic, *in vitro*, and *in vivo* studies might be necessary to establish the identity of causal loci.

Supplemental Data

Supplemental Data can be found online at <https://doi.org/10.1016/j.ajhg.2019.04.014>.

Acknowledgments

The authors thank the individuals who participated in this study and their families. We also thank Drs. Kenji Kurosawa, Seiji Mizuno, Hiroshi Kawame, Tsutomu Ogata, Yoichi Matsubara, and other physicians for sending samples of patients, and Ikumi Umeki, Yoko Tateda, Kumi Kato, Miyuki Tsuda, Mami Kikuchi, Makiko Nakagawa, and Kiyotaka Kuroda for their technical assistance. We also acknowledge the technical support of the Biomedical Research Core of Tohoku University Graduate School of Medicine. This work was supported by US National Institutes of Health grant MH106826 to E.E.D., AMED under grants to Y.A. (JP18ek0109241 and JP18ek0109278) and N.M. (JP18ek0109280, JP18dm0107090, JP18ek0109301, JP18ek0109348, and JP18kk020501), and Japan Society for the Promotion of Science (JSPS) KAKENHI Grant Numbers JP16K15522 to Y.A., JP17H01539 to N.M., JP17H06994 to A.F., and JP15KK0293 to T.N.

Declaration of Interests

N.K. is a paid consultant and holds founder stock in Rescindo Therapeutics. The other authors declare no competing interests.

(B) Quantification of the ceratohyal angle. Left: we injected 25 pg mRNA encoding each indicated *RRAS2* condition. $n = 61$ –80 embryos per batch. n.s., not significant; $**p < 0.001$ by Dunnett's test. Right: 5 pg of p.Gln72Leu encoding mRNA was injected. $n = 39$ –56 embryos per batch. $*p < 0.01$ by Student's *t* test. The thick line in the box represents median value; the bottom and top lines of the box represent first and third quartiles, respectively; the whiskers extend from the hinge to the lowest or highest value that is within 1.5-fold of interquartile range from the hinge; the filled circles are outliers.

(C) The body (lower arrow) and head (upper arrow) length were measured at 3 dpf. Representative images of an uninjected control (UI) and *RRAS2*-mRNA injected larvae are shown. Scale bar: 500 μ m.

(D and E) Quantification of body length (D) and relative head size, which was the value of the head length divided by the value of the body length (E). Left: we injected 25 pg of each *RRAS2* mRNA. $n = 61$ –82 embryos per batch. n.s., not significant; $**p < 0.001$ by Dunnett's test. Right: 5 pg of p.Gln72Leu encoding RNA was injected. $n = 36$ –53 embryos per batch. n.s., not significant by Student's *t* test. The thick line in the box represents median value; the bottom and top lines of the box represent first and third quartiles, respectively; the whiskers extend from the hinge to the lowest or highest value that is within 1.5-fold of interquartile range from the hinge; the filled circles are outliers.

Web Resources

1000 Genomes, <http://www.internationalgenome.org/>
CADD, <https://cadd.gs.washington.edu/>
COSMIC, <https://cancer.sanger.ac.uk/cosmic/gene/analysis?ln=RRAS2>
dbSNP, <https://www.ncbi.nlm.nih.gov/projects/SNP/>
ExAC Browser, <http://exac.broadinstitute.org/>
Human Genetic Variation Database (HGVD), <http://www.genome.med.kyoto-u.ac.jp/SnpDB/>
MutationTaster, <http://www.mutationtaster.org/>
OMIM, <http://www.omim.org/>
PolyPhen-2, <http://genetics.bwh.harvard.edu/pph2/>
PROVEAN, <http://provean.jcvi.org>
R statistical software, <https://www.r-project.org/>

References

- Aoki, Y., Niihori, T., Inoue, S., and Matsubara, Y. (2016). Recent advances in RASopathies. *J. Hum. Genet.* *61*, 33–39.
- Johnston, J.J., van der Smagt, J.J., Rosenfeld, J.A., Pagnamenta, A.T., Alswaid, A., Baker, E.H., Blair, E., Borck, G., Brinkmann, J., Craigen, W., et al.; Members of the Undiagnosed Diseases Network (2018). Autosomal recessive Noonan syndrome associated with biallelic LZTR1 variants. *Genet. Med.* *20*, 1175–1185.
- Tidyman, W.E., and Rauen, K.A. (2009). The RASopathies: developmental syndromes of Ras/MAPK pathway dysregulation. *Curr. Opin. Genet. Dev.* *19*, 230–236.
- Aoki, Y., Niihori, T., Narumi, Y., Kure, S., and Matsubara, Y. (2008). The RAS/MAPK syndromes: novel roles of the RAS pathway in human genetic disorders. *Hum. Mutat.* *29*, 992–1006.
- Aoki, Y., Niihori, T., Kawame, H., Kurosawa, K., Ohashi, H., Tanaka, Y., Filocamo, M., Kato, K., Suzuki, Y., Kure, S., and Matsubara, Y. (2005). Germline mutations in HRAS proto-oncogene cause Costello syndrome. *Nat. Genet.* *37*, 1038–1040.
- Niihori, T., Aoki, Y., Narumi, Y., Neri, G., Cavé, H., Verloes, A., Okamoto, N., Hennekam, R.C.M., Gillessen-Kaesbach, G., Wiczorek, D., et al. (2006). Germline KRAS and BRAF mutations in cardio-facio-cutaneous syndrome. *Nat. Genet.* *38*, 294–296.
- Schubbert, S., Zenker, M., Rowe, S.L., Böll, S., Klein, C., Bollag, G., van der Burgt, I., Musante, L., Kalscheuer, V., Wehner, L.E., et al. (2006). Germline KRAS mutations cause Noonan syndrome. *Nat. Genet.* *38*, 331–336.
- Rodriguez-Viciana, P., Tetsu, O., Tidyman, W.E., Estep, A.L., Conger, B.A., Cruz, M.S., McCormick, F., and Rauen, K.A. (2006). Germline mutations in genes within the MAPK pathway cause cardio-facio-cutaneous syndrome. *Science* *311*, 1287–1290.
- Tartaglia, M., Mehler, E.L., Goldberg, R., Zampino, G., Brunner, H.G., Kremer, H., van der Burgt, I., Crosby, A.H., Ion, A., Jeffery, S., et al. (2001). Mutations in PTPN11, encoding the protein tyrosine phosphatase SHP-2, cause Noonan syndrome. *Nat. Genet.* *29*, 465–468.
- Aoki, Y., Niihori, T., Banjo, T., Okamoto, N., Mizuno, S., Kurosawa, K., Ogata, T., Takada, F., Yano, M., Ando, T., et al. (2013). Gain-of-function mutations in RIT1 cause Noonan syndrome, a RAS/MAPK pathway syndrome. *Am. J. Hum. Genet.* *93*, 173–180.
- Gripp, K.W., Aldinger, K.A., Bennett, J.T., Baker, L., Tusi, J., Powell-Hamilton, N., Stabley, D., Sol-Church, K., Timms, A.E., and Dobyns, W.B. (2016). A novel rasopathy caused by recurrent de novo missense mutations in PPP1CB closely resembles Noonan syndrome with loose anagen hair. *Am. J. Med. Genet. A.* *170*, 2237–2247.
- Higgins, E.M., Bos, J.M., Mason-Suares, H., Tester, D.J., Ackerman, J.P., MacRae, C.A., Sol-Church, K., Gripp, K.W., Urrutia, R., and Ackerman, M.J. (2017). Elucidation of MRAS-mediated Noonan syndrome with cardiac hypertrophy. *JCI Insight* *2*, e91225.
- Chan, A.M., Miki, T., Meyers, K.A., and Aaronson, S.A. (1994). A human oncogene of the RAS superfamily unmasked by expression cDNA cloning. *Proc. Natl. Acad. Sci. USA* *91*, 7558–7562.
- Graham, S.M., Vojtek, A.B., Huff, S.Y., Cox, A.D., Clark, G.J., Cooper, J.A., and Der, C.J. (1996). TC21 causes transformation by Raf-independent signaling pathways. *Mol. Cell. Biol.* *16*, 6132–6140.
- Stieglitz, E., Taylor-Weiner, A.N., Chang, T.Y., Gelston, L.C., Wang, Y.D., Mazor, T., Esquivel, E., Yu, A., Seepo, S., Olsen, S., et al. (2015). The genomic landscape of juvenile myelomonocytic leukemia. *Nat. Genet.* *47*, 1326–1333.
- Prior, I.A., Lewis, P.D., and Mattos, C. (2012). A comprehensive survey of Ras mutations in cancer. *Cancer Res.* *72*, 2457–2467.
- Graham, S.M., Cox, A.D., Drivas, G., Rush, M.G., D'Eustachio, P., and Der, C.J. (1994). Aberrant function of the Ras-related protein TC21/R-Ras2 triggers malignant transformation. *Mol. Cell. Biol.* *14*, 4108–4115.
- van der Burgt, I. (2007). Noonan syndrome. *Orphanet J. Rare Dis.* *2*, 4.
- Huang, Y., Saez, R., Chao, L., Santos, E., Aaronson, S.A., and Chan, A.M. (1995). A novel insertional mutation in the TC21 gene activates its transforming activity in a human leiomyosarcoma cell line. *Oncogene* *11*, 1255–1260.
- Rong, R., He, Q., Liu, Y., Sheikh, M.S., and Huang, Y. (2002). TC21 mediates transformation and cell survival via activation of phosphatidylinositol 3-kinase/Akt and NF-kappaB signaling pathway. *Oncogene* *21*, 1062–1070.
- Inoue, S., Moriya, M., Watanabe, Y., Miyagawa-Tomita, S., Niihori, T., Oba, D., Ono, M., Kure, S., Ogura, T., Matsubara, Y., and Aoki, Y. (2014). New BRAF knockin mice provide a pathogenetic mechanism of developmental defects and a therapeutic approach in cardio-facio-cutaneous syndrome. *Hum. Mol. Genet.* *23*, 6553–6566.
- Tsai, I.C., McKnight, K., McKinstry, S.U., Maynard, A.T., Tan, P.L., Golzio, C., White, C.T., Price, D.J., Davis, E.E., Amrine-Madsen, H., and Katsanis, N. (2018). Small molecule inhibition of RAS/MAPK signaling ameliorates developmental pathologies of Kabuki Syndrome. *Sci. Rep.* *8*, 10779.
- Bögershausen, N., Tsai, I.C., Pohl, E., Kiper, P.O., Beleggia, F., Percin, E.F., Keupp, K., Matchan, A., Milz, E., Alanay, Y., et al. (2015). RAP1-mediated MEK/ERK pathway defects in Kabuki syndrome. *J. Clin. Invest.* *125*, 3585–3599.
- Magini, P., Pippucci, T., Tsai, I.C., Coppola, S., Stellacci, E., Bartoletti-Stella, A., Turchetti, D., Graziano, C., Cenacchi, G., Neri, I., et al. (2014). A mutation in PAK3 with a dual molecular effect deregulates the RAS/MAPK pathway and drives an

- X-linked syndromic phenotype. *Hum. Mol. Genet.* 23, 3607–3617.
25. Hutson, M.R., Keyte, A.L., Hernández-Morales, M., Gibbs, E., Kupchinsky, Z.A., Argyridis, I., Erwin, K.N., Pegram, K., Kneifel, M., Rosenberg, P.B., et al. (2017). Temperature-activated ion channels in neural crest cells confer maternal fever-associated birth defects. *Sci. Signal.* 10, 10.
 26. Runtuwene, V., van Eekelen, M., Overvoorde, J., Rehmann, H., Yntema, H.G., Nillesen, W.M., van Haeringen, A., van der Burgt, I., Burgering, B., and den Hertog, J. (2011). Noonan syndrome gain-of-function mutations in NRAS cause zebrafish gastrulation defects. *Dis. Model. Mech.* 4, 393–399.
 27. Gelb, B.D., Cavé, H., Dillon, M.W., Gripp, K.W., Lee, J.A., Mason-Suares, H., Rauen, K.A., Williams, B., Zenker, M., Vincent, L.M.; and ClinGen RASopathy Working Group (2018). ClinGen's RASopathy Expert Panel consensus methods for variant interpretation. *Genet. Med.* 20, 1334–1345.
 28. Jopling, C., van Geemen, D., and den Hertog, J. (2007). Shp2 knockdown and Noonan/LEOPARD mutant Shp2-induced gastrulation defects. *PLoS Genet.* 3, e225.
 29. Santoriello, C., Deflorian, G., Pezzimenti, F., Kawakami, K., Lanfranccone, L., d'Adda di Fagagna, F., and Mione, M. (2009). Expression of H-RASV12 in a zebrafish model of Costello syndrome causes cellular senescence in adult proliferating cells. *Dis. Model. Mech.* 2, 56–67.
 30. Vissers, L.E., Bonetti, M., Paardekooper Overman, J., Nillesen, W.M., Frints, S.G., de Ligt, J., Zampino, G., Justino, A., Machado, J.C., Schepens, M., et al. (2015). Heterozygous germline mutations in A2ML1 are associated with a disorder clinically related to Noonan syndrome. *Eur. J. Hum. Genet.* 23, 317–324.
 31. Anastasaki, C., Estep, A.L., Marais, R., Rauen, K.A., and Patton, E.E. (2009). Kinase-activating and kinase-impaired cardio-facio-cutaneous syndrome alleles have activity during zebrafish development and are sensitive to small molecule inhibitors. *Hum. Mol. Genet.* 18, 2543–2554.
 32. Capri, Y., Flex, E., Krumbach, O.H.F., Carpentieri, G., Ceccetti, S., Lißewski, C., Adariani, S.R., Schanze, D., Brinkmann, J., Piard, J., et al. (2019). Activating mutations of RRAS2 are a rare cause of Noonan syndrome. *Am. J. Hum. Genet.* 104, this issue, 1223–1232.

Supplemental Data

Germline-Activating *RRAS2* Mutations

Cause Noonan Syndrome

Tetsuya Niihori, Koki Nagai, Atsushi Fujita, Hirofumi Ohashi, Nobuhiko Okamoto, Satoshi Okada, Atsuko Harada, Hirotaka Kihara, Thomas Arbogast, Ryo Funayama, Matsuyuki Shirota, Keiko Nakayama, Taiki Abe, Shin-ichi Inoue, I-Chun Tsai, Naomichi Matsumoto, Erica E. Davis, Nicholas Katsanis, and Yoko Aoki

Supplemental Note: a case report

HU1 was a boy and the third child of healthy non-consanguineous parents. Polyhydramnios and enlargement of cerebral ventricles were pointed out in his gestational period. He was born at 36 weeks of gestational age by vaginal delivery. His body weight, body length, and head circumference at birth were 2,644 g ($-0.31SD$), 49.0 cm ($+0.83SD$), and 37.7 cm ($+3.8SD$), respectively. He had respiratory distress due to hypotonia and respiratory care was initiated by nasal directional positive airway pressure. Oxygenation was continued by 31 days of age. He had macrocephaly, low set ears, micrognathia, unilateral cryptorchidism, hydrocele testicle, and micropenis. On the other side, no obvious pulmonary artery stenosis and lymphatic malformation were pointed out. Trans-fontanel ultrasonography showed an enlargement of ventricles. His chromosomal G-banding and microarray analysis were normal. At the age of 5 months, analyses of organic acids, acylcarnitine, and very long chain fatty acids were normal. At the same age, he started tube feeding because he had a gastroesophageal reflux leading to a respiratory disease. A head magnetic resonance imaging at age 6 months showed enlargement of his lateral, third, and fourth ventricles but no Chiari malformations. His brain myelination was equivalent to that expected for a 4-month-old infant (Fig. 1K). He had a gastrostomy at the age of 13 months and a ventriculoperitoneal shunt surgery at age 14 months. At the

age of 14 months, eosinophilia and eosinophils in stool were found, suggesting the presence of a milk allergy. After the age of 2 years and 2 months, vomiting persisted and he had a ketotic hypoglycemia (blood glucose 29 mg/dL, acetoacetic acid 196 μ mol/L; normal < 55 μ mol/L, 3-hydroxybutyric acid 108 μ mol/L; normal < 85, NH₃ 40 μ g/dL; normal 30–86 μ g/dL) at age 2 years and 3 months. The laboratory test data on admission showed elevated brain natriuretic peptide (BNP, 798 pg/mL; normal < 18.4 pg/mL) and decreased insulin-like growth factor 1 (< 4 ng/mL; normal 24–164 ng/mL). Echocardiography revealed cardiac hypofunction without the findings of hypertrophic or dilated cardiomyopathy. Adenovirus 41 was detected by virus isolation from his urine and stool. The cardiac hypofunction persisted after this infectious episode. At the age of 3 years 0 month, he had clinical signs suggesting infection such as hard breathing, cough, and rhinorrhea. His white blood cell count and C-reactive protein were slightly elevated. His respiratory disease got worse during 4 days, and he was hospitalized. BNP on admission was 586 pg/mL. Ultrasound imaging showed marked dilation of left ventricle and contractile dysfunction. After three days of admission, he died of cardiac failure in spite of mechanical ventilation and administration of catecholamines in an intensive care unit. He had severe failure to thrive and developmental delay throughout his life. At age 3 years, his body weight, body length, and head circumference were 6,145

g (-5.0 SD), 72.5 cm (-5.9 SD), and 51.0 cm (-0.1 SD), respectively. He was able to smile, pursue something visually, and shake his head, but not to control his head.

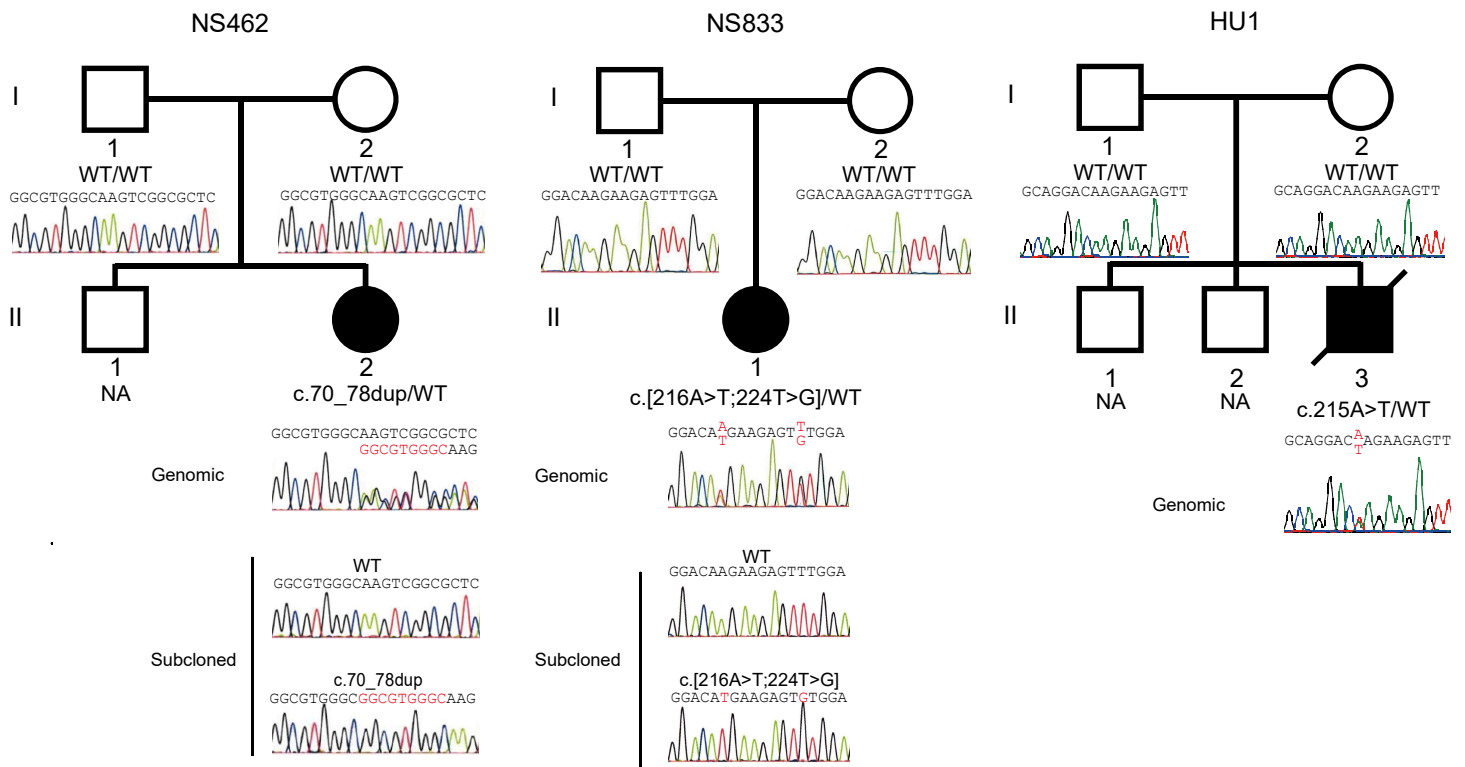


Figure S1. Sanger sequencing of *de novo* variants in *RRAS2* identified in individuals with Noonan syndrome (NS)

Four *de novo* variants in *RRAS2* were identified in three individuals with NS. PCR products amplified using genomic DNA from peripheral blood of individuals NS462 (II-2) and NS833 (II-1) were subcloned into pCR4 TOPO vector and sequenced. Subcloned sequence of NS833 shows that the two variants were on the same chromosome. Abbreviations: WT, wide-type; and NA, not available

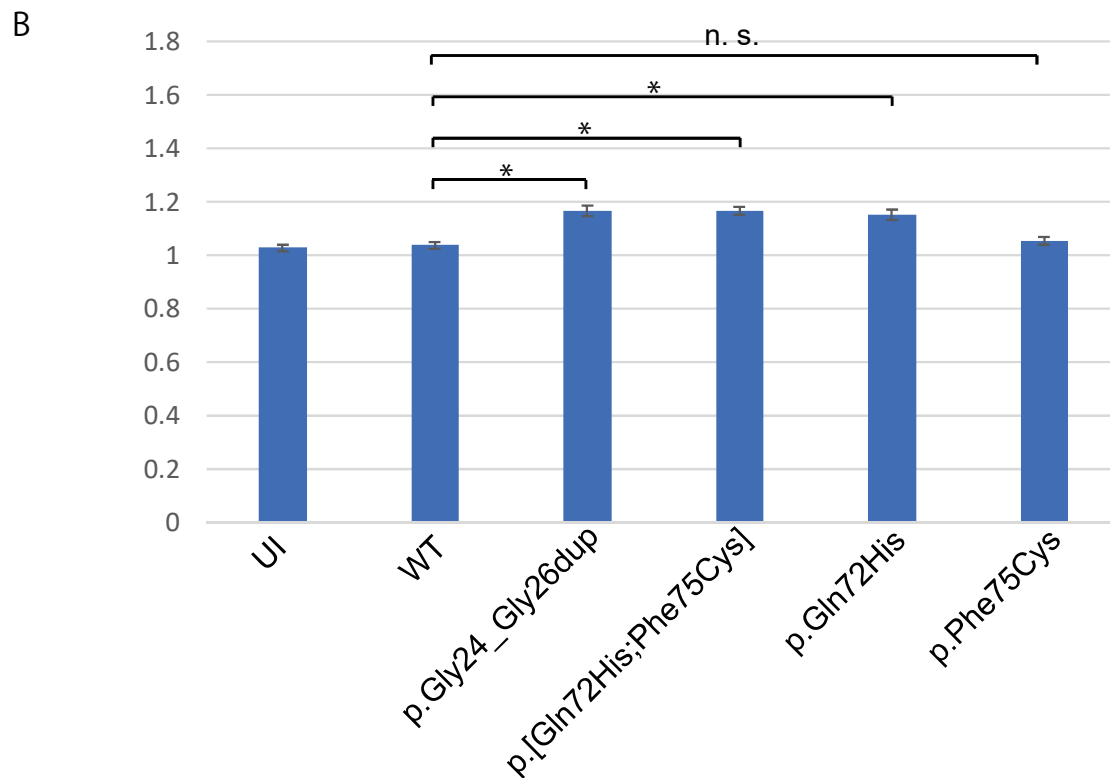
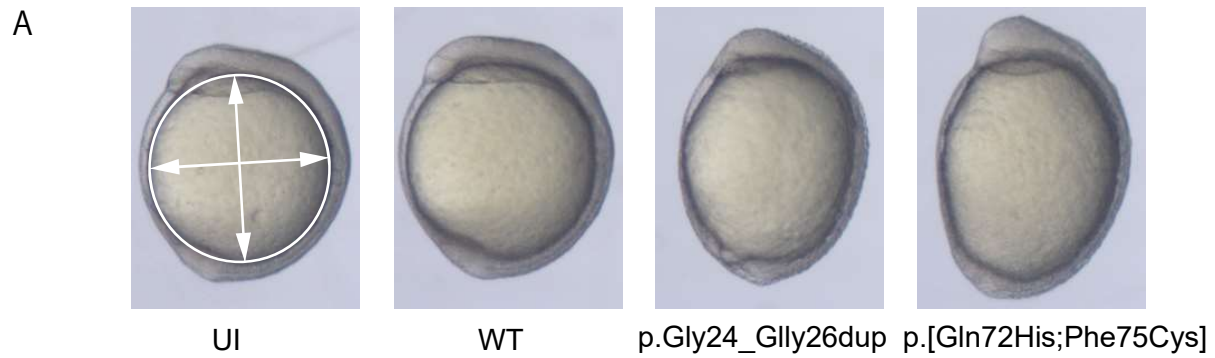
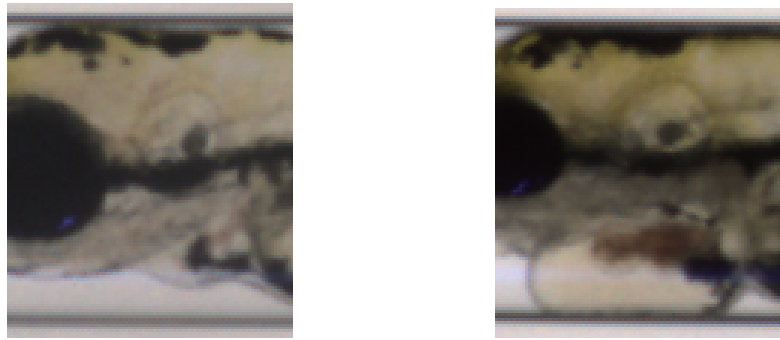


Figure S2. Morphology of zebrafish embryos injected with wild-type (WT) or mutant *RRAS2* mRNA at 11 hpf

(A) Embryos were injected at the 1–4 cell stages with synthetic RNA (25 pg) encoding *RRAS2* (wild-type or mutant) and morphology was assessed at 11 hpf. The major and minor axes (pointed by axes) of the yolk were measured using Image J. Representative batches of embryos are depicted. (B) Quantification of the ratio of the major and minor axes upon injection with synthetic RNAs encoding WT or mutant *RRAS2* as indicated. n = 76–85 embryos per batch. Error bars represent standard errors of the mean. n.s., not significant;

*: P < 0.001

A



B

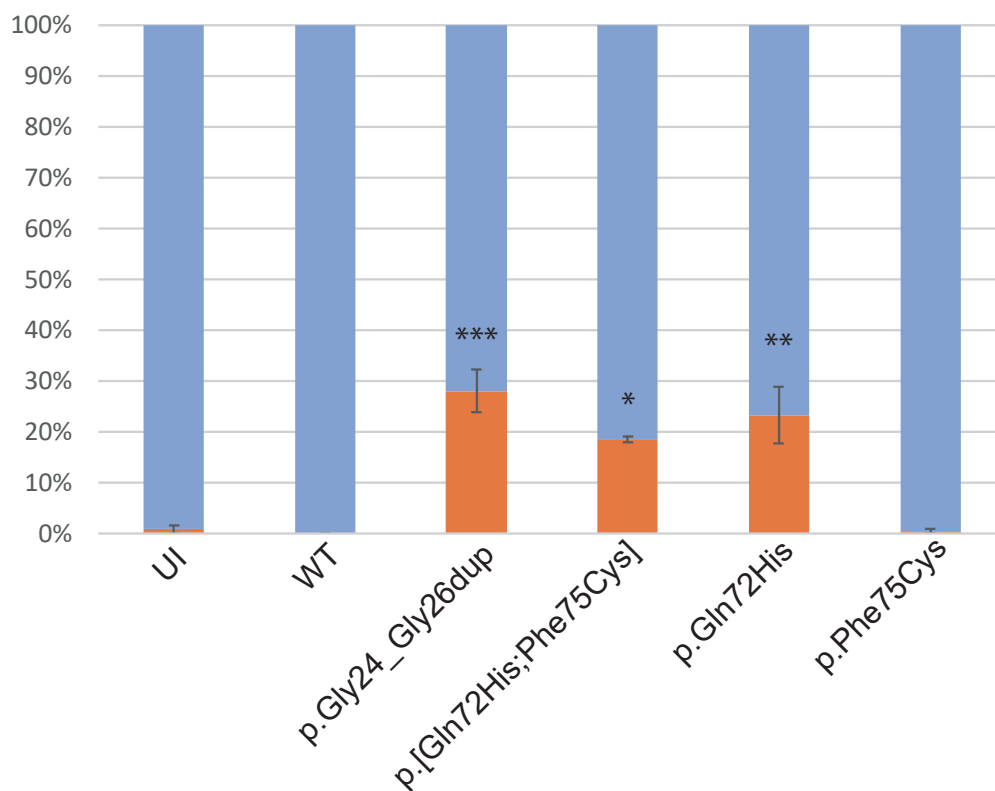


Figure S3. Pericardial edema of zebrafish embryos injected with wild-type (WT) or mutant *RRAS2* mRNA at 3 days post fertilization (dpf)

(A) Representative image of larvae at 3 dpf. Left panel: normal morphology of pericardium. Right panel:

pericardial edema. (B) Ratio of larvae with pericardial edema. Experiments were repeated three times and the mean percentages of larvae with pericardial edema were shown. $n = 32-86$ larvae per batch.

Error bars show standard errors of the mean. ***: $P < 0.001$; **: $P < 0.01$; *: $P < 0.05$, compared with WT.

Table S2. *In Silico* predictions of *RRAS2* variants in individuals with NS.

Chr	Position	Ref	Alt	Nucleotide change (NM_012250.5)	Amino acid change (NP_036382.2)	PROVEAN	Mutation Taster	Polyphen-2 (Humdiv)	CADD >30
11	14,380,338	-	GCCCACGCC	c.70_78dup	p.Gly24_Gly26dup	Deleterious	polymorphism	-	No (17.69)
11	14,316,389	T	A	c.216A>T	p.Gln72His	Deleterious	disease causing	Probably damaging	No (27.1)
11	14,316,390	T	A	c.215A>T	p.Gln72Leu	Deleterious	disease causing	Possibly damaging	No (28.4)
11	14,316,381	A	C	c.224T>G	p.Phe75Cys	Deleterious	disease causing	Probably damaging	Yes (31)

Table S3. Primer pairs used to amplify coding exons and their flanking introns in *RRAS2*

Flagment	Exon	Forward	Reverse
1	1 ^a	5'-F-gtttcattctctgccagcca	5'-R-tagagtggagagggagatgc
2	1 ^b	5'-F-tcatgcatatgcagcacctca	5'-R-gaccacattcctgagaagc
3	2 ^{a,b}	5'-F-gcctcaagtgatccttctc	5'-R-catgggctaattccagatc
4	3 and 4 ^{a, b, c}	5'-F-gctctctagaggactcaca	5'-R-cacttaagtggcatggagc
5	5 ^{a,b, c}	5'-F-aaacaacttggcctttggc	5'-R-ccctagaaaggaatcacttc
6	6 ^{a,b, c}	5'-F-ggaaagagagaaattccctcg	5'-R-ggctagaaaggtaccaacaag

a, in NM_001177314.1; b, in NM_012250.5; c, in NM_001177315.1 and NM_001102669.2; F, 5'- gtaaacgacggccagt; R, 5'- aggaaacagctatgacc. Exons 1 and 2 of NM_001177315.1 and NM_001102669.2 were non-coding exons.

Supplemental Materials and Methods

Genetic analysis

This study was approved by the Ethics Committee of the Tohoku University School of Medicine. Written informed consent was obtained from all subjects involved in the study or from their parents. This study included 27 individuals for WES and 191 individuals for Sanger sequencing with suspected NS or related disorders who were not found to harbor a mutation based on Sanger sequence screening, which included *PTPN11* (exons 1–15), *SHOC2* (exon 1), *KRAS* (exons 1–5), *RAF1* (exons 7, 14, and 17), *HRAS* (exons 1–5), *BRAF* (exons 6 and 11–16), *MAP2K1* (exons 2 and 3), *MAP2K2* (exons 2 and 3), *SOS1* (exons 1–23), and *RIT1* (exons 1–6). We extracted DNA from peripheral blood according to standard procedures, from hair and fingernails using IsoHair (Nippon Gene, Tokyo, Japan), and/or from saliva using Oragene (DNA Genotek, Ottawa, Ontario, Canada). Libraries for WES were prepared using the SureSelect Human All Exon Kit Ver 4 (NS462) or Ver 6 (NS833 and others) (Agilent technologies, Santa Clara, CA, USA). Libraries were sequenced for 101 (NS462) or 126 (NS833 and others) bases with paired-ends on Hiseq 2500 (Illumina, San Diego, CA, USA). Mapping, variant calls, and annotations were performed as described¹. WES on DNAs from HU1 and his parents were performed as described previously². Microarray

analysis of DNA from the peripheral blood samples of NS462 was performed using CytoScan HD array (Affymetrix, Santa Clara, CA, USA). Sanger sequencing was performed as described³ using primers listed in Supplemental Table 3.

Plasmid construction and site-direct mutagenesis

We generated human *RRAS2* cDNA by RT-PCR using human leukocyte cDNA as a template. The human *RRAS2* ORF (NM_012250.5) was amplified by PCR using a forward primer containing a *Bam*HI site and a reverse primer containing an *Eco*RI site. The amplified fragment was digested with *Bam*HI and *Eco*RI and cloned into pCS2+. Mutagenesis was performed using a QuickChange Lightning Site-Directed Mutagenesis Kit (Agilent Technologies). All vectors were confirmed by Sanger sequencing.

Active RAS pull-down assay and immunoblotting

To evaluate binding between RBD and *RRAS2*, we performed a RAS pull-down assay. The RAS Assay Reagent (RAF-1 RBD agarose, #14-278) was purchased from Millipore (Burlington, MA, USA). HEK293 cells were plated in 6-cm dishes at 5×10^5 cells per well and maintained in Dulbecco's Modified Eagle Medium (DMEM) containing 10% fetal bovine serum, 100 U/mL penicillin, and 100 μ g/mL streptomycin. Twenty-four

hours later, cells were transfected using Lipofectamine 3000 (Invitrogen, Waltham, MA, USA) with 5 µg WT or mutant *RRAS2* construct. The next day, medium was replaced by serum-free DMEM. Cells were harvested after serum starvation for 24 hours. The pull-down assay was performed according to the manufacturer's protocol of the RAS Activation Assay kit (#17-218, Millipore) using lysis/wash buffer (25 mM Tris/HCl pH8.0, 150 mM NaCl, 5 mM MgCl₂, 1% Nonidet P-40, 0.25% sodium deoxycholate, and 5% glycerol) instead of Mg²⁺ Lysis/Wash Buffer (# 20-168, Millipore). RAF-1 RBD agarose beads after pull-down reaction and cell lysates were mixed with 4x Laemmli sample buffer (Biorad, Hercules, CA, USA) and boiled at 95 °C for 5 minutes. Electrophoresis was performed on 5-20% gradient gels (E-R520L, ATTO, Tokyo, Japan). Antibodies against RRAS2 (PA5-22123, Thermo Fisher Scientific, Waltham, MA, USA), p44/42 MAPK (#9102, Cell Signaling Technology (CST), Danvers, MA, USA), phospho-p44/42 MAPK (#9101, CST), MEK1/2 (#8727, CST), phospho-MEK1/2 (#9154, CST), AKT(#9272, CST), phospho-AKT (#9272 for Ser473 and #2965 for Thr308, CST) and β-actin (A5316, Sigma, St. Louis, MO, USA) were used for immunoblotting. All experiments were performed in triplicates. Intensities of suggested molecules were quantified with Image J. Statistical analyses were performed by Dunnett's test using the multcomp package of R_3.5.1.

Luciferase assay

We performed a reporter assay to determine the effect on downstream of RAS/MAPK signaling pathway. HEK293 cells were plated in 24-well plates at 5×10^4 cells per well. After 24 hours, cells were transfected transiently with 300 ng pFR-luc, 15 ng pFA2-ELK1, 10 ng phRLnull-luc, and 50 ng WT or mutant *RRAS2* construct using Lipofectamine 3000 (Invitrogen). After 18 hours, cells were serum starved in DMEM for 24 hours. Cells were then harvested in passive lysis buffer, and luciferase activity was assayed using the Promega Dual-Luciferase Assay Kit (Promega, Madison, WI, USA). Renilla luciferase expressed by phRLnull-luc was used to normalize transfection efficiency. The experiments were performed using three wells in each condition. Statistical analyses were performed by Dunnett's test using the multcomp package of R_3.5.1.

Zebrafish embryos

All zebrafish-related experiments were performed in accordance with protocols approved by the Duke University Institutional Animal Care and Use Committee.

Zebrafish embryos were obtained by natural mating of transgenic (*-1.4coll1a1:egfp⁴*) adults on AB background and were maintained at 28°C on a 14 h/10 h light/dark cycle.

RNA injections in zebrafish

pCS2+ constructs of WT and variant *RRAS2* were linearized with *NotI*, and capped mRNA was transcribed with the mMessage mMachine SP6 Kit (Thermo Fisher) according to the manufacturer's instructions. Approximately 1 nL cocktail of 5 or 25 ng/ μ L RNA and 0.2% phenol red were injected into yolks of embryos at the 1–4 cell stage. At 11 hpf, we obtained images of embryos to determine yolk elongation. At 3 dpf, larval batches were anesthetized with 0.2 mg/mL Tricaine and imaged using the Vertebrate Automated Screening Technology Bioimager (VAST, Union Biometrica, Holliston, MA, USA). We obtained fluorescent images of GFP-positive cells on ventrally positioned larvae and dorsal and lateral brightfield images of whole larvae using VAST. Phenotypic analyses (measuring length of the major and minor axes of embryos at 11 hpf and length of body and head at 3 dpf) were performed using Image J. Statistical analyses were performed by Dunnett's test using the multcomp package of R_3.5.1. or Student's t test using Excel.

References

1. Niihori, T., Ouchi-Uchiyama, M., Sasahara, Y., Kaneko, T., Hashii, Y., Irie, M., Sato, A., Saito-Nanjo, Y., Funayama, R., Nagashima, T., et al. (2015). Mutations in MECOM, Encoding Oncoprotein EVI1, Cause Radioulnar Synostosis with Amegakaryocytic Thrombocytopenia. *Am J Hum Genet* 97, 848-854.
2. Hamanaka, K., Miyatake, S., Zerem, A., Lev, D., Blumkin, L., Yokochi, K., Fujita, A., Imagawa, E., Iwama, K., Nakashima, M., et al. (2018). Expanding the phenotype of IBA57 mutations: related leukodystrophy can remain asymptomatic. *J Hum Genet* 63, 1223-1229.
3. Niihori, T., Aoki, Y., Okamoto, N., Kurosawa, K., Ohashi, H., Mizuno, S., Kawame, H., Inazawa, J., Ohura, T., Arai, H., et al. (2011). HRAS mutants identified in Costello syndrome patients can induce cellular senescence: possible implications for the pathogenesis of Costello syndrome. *J Hum Genet* 56, 707-715.
4. Kague, E., Gallagher, M., Burke, S., Parsons, M., Franz-Odenaal, T., and Fisher, S. (2012). Skeletogenic fate of zebrafish cranial and trunk neural crest. *PLoS One* 7, e47394.